Angewandte Chemie
Eine Zeitschrift der Gesellschaft Deutscher Chemiker

Supporting Information

© Wiley-VCH 2008

69451 Weinheim, Germany

SUPPORTING ONLINE MATERIAL

Functionalized nanocompartments (Synthosomes) with a reduction-triggered release system

*Ozana Onaca[1], Pransenjit Sarkar[1], Danilo Roccatano[1], Thomas Friedrich[2], Bernard Hauer[2], Mariusz Grzelakowski[3], Arcan Güven[1], Marco Fioroni[1] and Ulrich Schwaneberg[1]**

1) School of Engineering and Science
Jacobs University
Campus Ring 8, 28759, Bremen, Germany
* To whom correspondence should be addressed: E-mail: u.schwaneberg@jacobs-university.de

2) BASF AG
Fine Chemicals and Biocatalysis Research
GVF/D-A030, 67056, Ludwigshafen, Germany

3) M. Grzelakowski
Department of Chemistry
University of Basel
Klingelbergstrasse 80, CH-4056 Basel, Switzerland

Experimental procedures

All chemicals used were of analytical reagent grade or higher quality and purchased from Sigma-Aldrich Chemie (Taufkirchen, Germany) and Applichem (Darmstadt, Germany) if not stated otherwise. FhuA Δ1-160 variant was expressed, extracted and purified as previously described [2] until homogeneity using *E. coli* B^E strain BL 21 (DE3) omp8 (F^- *hsdS*$_B$ (r_B^- m_B^-) *gal ompT dcm* (DE3) Δ*lamB ompF*::Tn*5* Δ*ompA* Δ*ompC*) [24]. Protein concentrations were determined using the standard BCA kit (Pierce Chemical Co, Rockford, USA).

FhuA Δ1-160 labeling and nanocompartment formation

A 20 % DMSO aqueous solution containing 3-(2-pyridyldithio) propionic acid N-hydroxysuccinimide ester (76.8 mM) or (2-[Biotinamido]ethylamido)-3,3′-dithiodipropionic acid N-hydroxysuccinimide ester (8.2 mM) was added drop-wise to a FhuA Δ1-160 (50 µL, 4 µM) solution and stirred (3000 rpm, 1 h; RCT basic IKAMAG, IKA-Werke GmbH, Staufen,

Germany). The latter solution was used for formation of nanocompartments loaded with calcein (50 mM) according to a previously reported Ethanol method [2] without further work-up.

ABA (PMOXA-PDMS-PMOXA) triblock copolymer (50 mg; Mw ~20000 g/mol) was dissolved in ethanol (250 µl; 99.8 %) and stirred for 30 min. The clear solution was added drop-wise into Tris-KCl buffer (5 ml; 10 mM Tris, 100 mM KCl, pH 7.4) containing calcein (50 mM) and stirred (3000 rpm; ambient temperature; 3-4 h). Nanocompartments loaded with calcein (50 mM), harboring FhuA Δ1-160 (0.13 µM final concentration) as well as amino group labeled FhuA Δ1-160 (0.13 µM final concentration) were prepared as previously described using the Ethanol method and identical concentrations and volumes [2]. Nanocompartments formed by self-assembly were subsequently extruded (6 times; 0.22 µm Milex filter (Millipore Corporation, Bedford, MA, USA)) to form uniform spherically shaped nanocompartments [25].

Nanocompartments were purified by gel filtration using Sepharose 4B (Sigma-Aldrich) in 0.1 M phosphate buffer (PB), pH 7.6, 0.2 M sodium dihydrogen phosphate monohydrate (H_2NaO_4P) (39 ml) + 0.2 M di-sodium hydrogen phophate (anhydrous) (HNa_2O_4P) (261 ml) + 300 ml dH_2O. Average diameters of nanocompartments were routinely determined using a Zeta-Sizer (Zeta-Sizer Nano Series; Malvern, Worcestershire, United Kingdom).

Calcein release assay with Synthosomes

An excitation wavelength of 480 nm and an emission wavelength of 520 nm were used for all calcein release measurements. Fast kinetics were recorded for 15 minutes (kinetic interval 1 µs) using a Cary Eclipse Fluorescence Spectrophotometer (Varian, Inc. Corporate Headquarters, Palo Alto, USA). For measurements up to 120 minutes a Saphire Fluorescence Spectrophotometer (Tecan Trading AG, Mannedorf/Zurich, Switzerland) was employed (kinetic interval 60 s). In fast kinetic measurements a purified nanocompartment or Synthosome suspension (500 µl; Tris-KCl buffer (5 ml; 10 mM Tris, 100 mM KCl, pH 7.4) was supplemented with DTT (10 µl, 1 M), mixed gently by pipetting (Eppendorf, Hamburg, Germany), and used in

each experiment. Subsequently, 500 µl of a suspension were rapidly transferred into quartz cuvettes (Hellma GmbH&Co. KG, Müllheim, Germany) for recording calcein release kinetics.

For long time measurements 200 µl of a chromatographically purified nanocompartment or Synthosome suspension was supplemented with DTT (10 µl, 1 M) in a microtiter plate (Flat-Bottom, Black, 96 well, Greiner Bio-One, Frikenhausen, Germany), mixed with a pipette (Eppendorf, Hamburg, Germany), and used in each experiment. Integrity of nanocompartments and Synthosomes was determined by comparing size distribution and intensity via dynamic light scattering using a Zeta-Sizer (Zeta-Sizer Nano Series; Malvern, Worcestershire, United Kingdom) and TEM images (Fig. S1).

Polymersomes TEM, SLS and DLS Data

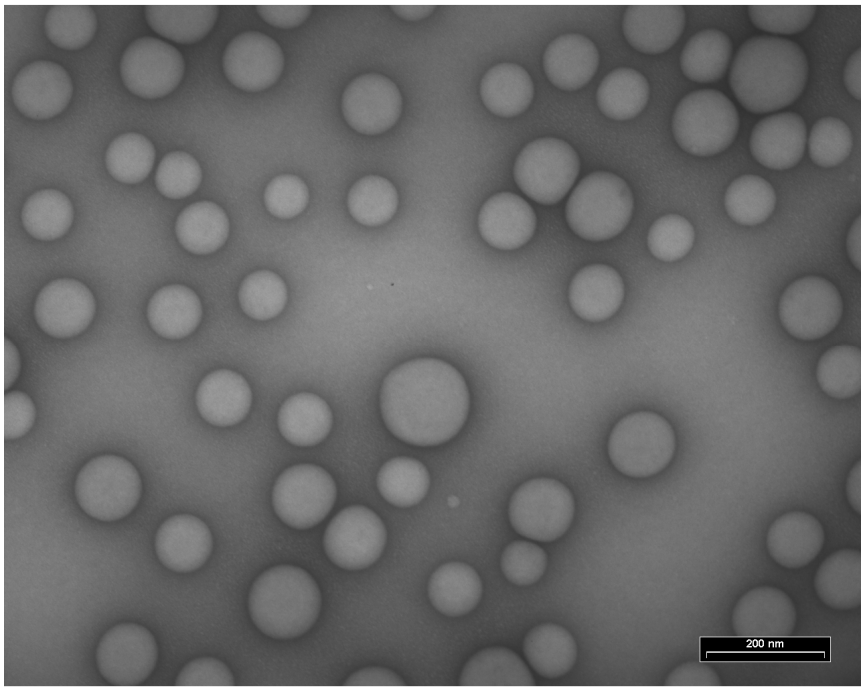

Fig. S1 TEM image of the PMOXA-PDMS-PMOXA polymersomes

Transmission Electron Microscopy (TEM) coupled with Static and Dynamic Light Scattering (SLS and DLS) measurements were performed to check the polymersomes integrity and average radii. The stability and vesicular nature of the triblock copolymer PMOXA-PDMS-

PMOXA has been already published[27]. Fig. S1 shows a TEM image of the polymersome present in solution. Accomplishing the TEM images, SLS and DLS techniques have been used to follow a systematic study of the average vesicle dimensions at different polymer (vesicle) concentrations (results are reported at the end of the Supporting Info section). The average polymer vesicle diameter was **208 nm**.

Blocking-Deblocking Chemistry

The blocking and deblocking chemistry is based on the NHS esters (N-hydroxysuccinimide) as active acylating reagents[28]. The comprehensive blocking reaction scheme is:

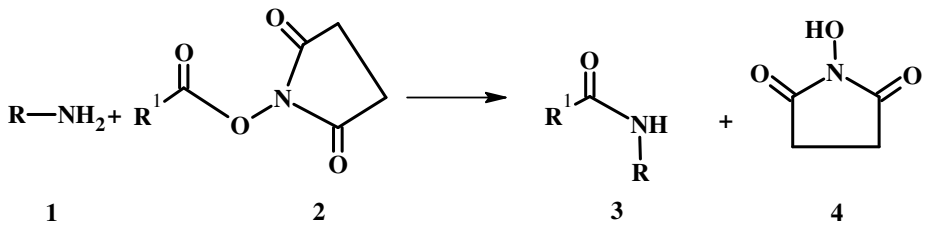

where an amine compound 1 (in our case a free amino group of the Lys residues) reacts with an NHS ester derivative 2, resulting in product 3 containing an amide bond (with R^1 being a Lys aminoacid bonded to the protein) and the leaving group NHS. The selected NHS ester derivatives were:

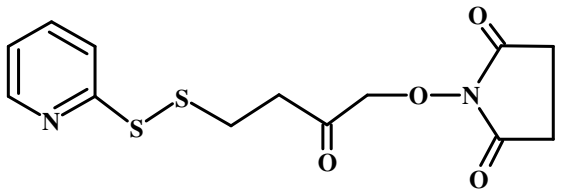

3-(2-pyridyldithio)propionic-acid-N-hydroxysuccinimide-ester

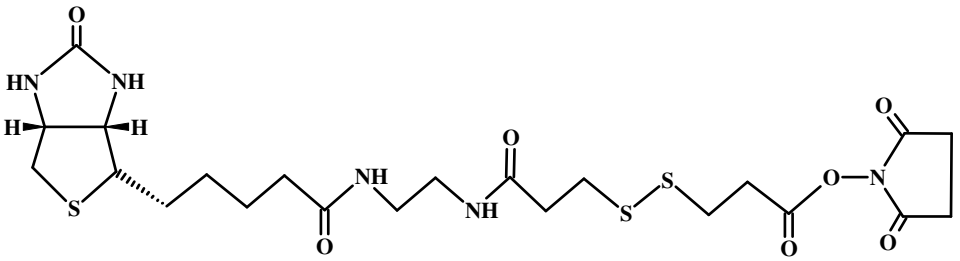

2-[biotinamido]ethylamido)-3,3′-dithiodipropionic acid N-hydroxysuccinimide ester

because of the presence of a disulfide bond which can be cleaved by DTT (dithiothreitol) addition; the general deblocking reaction scheme is:

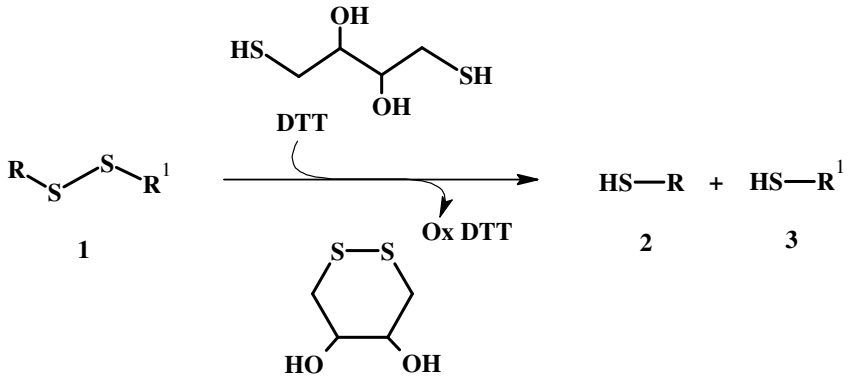

where a disulfide containing molecule 1; the NHS esters of the biotin and pyridyl residues; is reduced by DTT giving product reaction compounds 2 and 3. Two represents the pyridyl- or biotinyl-based leaving group while 3 is the remaining sulfhydryl group on the Lys residue bonded to the protein, i.e.

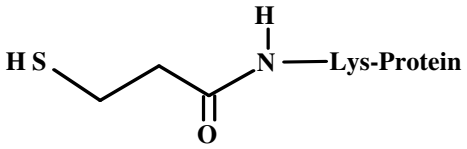

<u>CD Spectra of the free, biotinylated and de-biotinylated FhuA Δ1-160</u>

Circular dichroic (CD) spectra were registered on different samples to understand the effect of the blocking/deblocking chemistry on the protein secondary structure stability. Fig. S2 shows the CD spectra of the free FhuA Δ1-160 (full line), biotinylated (dashed) and de-biotinylated after DTT reaction (dot-dashed) are shown. The DICHROPROT 2000[29] program was used to calculate the secondary structure percentage using the least square method. In all the three samples a defined minima at 218 nm, typical of a β-sheet conformation is present, with a very good overlap between the not biotinylated and de-biotinylated FhuA Δ1-160, while the biotinylated shows a slight blue-shift at low wavelengths. This small difference is reasonably due to the presence of the biotinyl groups on the FhuA Δ1-160 protein[30].

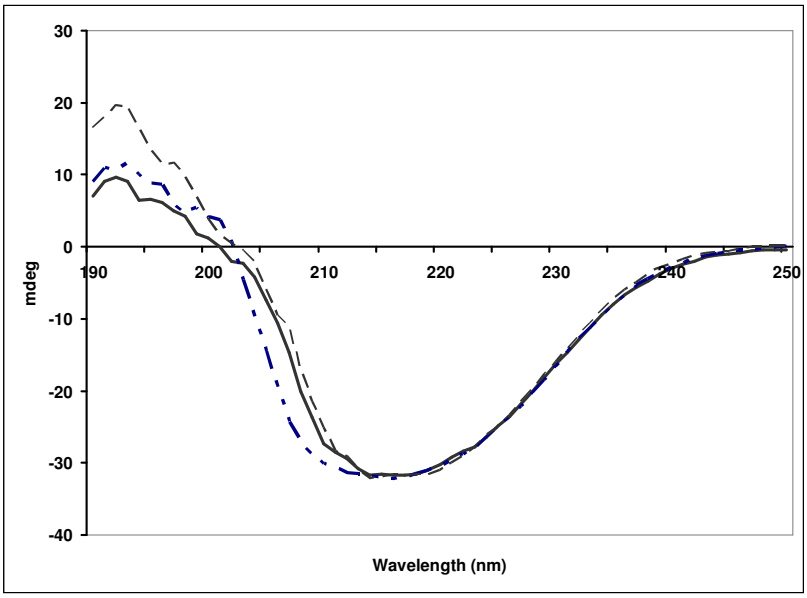

Fig. S2 CD spectra of the FhuA Δ1-160 not biotinylated (full line), biotinylated (dashed) and de-biotinylated after DTT reduction (dot-dashed)

The amount of β-structure, in all three samples is quite similar (49 %, 48 %, 52 %), showing a little effect of the selected chemistry after introducing and cleaving the biotinyl groups to the protein structure. The amount of β-sheet in the wild type FhuA is 51 %[31].

Quantitative determination of the biotinylated Lys (biotinylation Assay)

The determination of the biotinyl groups present on the FhuA protein has been performed using the Invitrogen FluoReporter® Biotin Quantitation Assay Kit specifically developed for proteins. Fluorescence spectra were detected by a Saphire Fluorescence Spectrophotometer (Tecan Trading AG, Mannedorf/Zurich, Switzerland). Important notice: do not use Tris buffer. The amino groups in the Tris will interfere with the biotinylation reaction being biotinylated itself! In the FhuA Δ1-160 mutant, there are 29 accessible Lys groups. Ten of these are of relevance for the channel of FhuA Δ1-160: 6 are buried in the channel and 4 are present on both ores of the channel. After biotinylation, two samples of the same batch were used: the first one was digested by proteases to expose all the buried biotinylated Lys, while the second one with the integer FhuA Δ1-160, was reduced by DTT. In the first experiment the biotinylation efficiency

was deduced while from the second one, the efficiency of the DTT reaction was calculated by the biotinyl molecules amount present in the washing solution after column separation. The obtained average amount of biotinyl groups for single FhuA Δ1-160 is 3.6. 80% of the fluorescence was recovered in the elute solution after DTT reduction proving that the DTT reduction works efficiently.

Molecular Modelling. Construction of Labeled Models

The crystal structure the FhuA enzyme (PDB entry 1BY3) [32] was obtained from the Protein Data Bank (www.pdb.org). The residues 1-160, forming the channel plug, were removed from the structure. The initial 3D structure for the pyridyl- and biotin-labeled fragments were constructed using the program ADC/ChemSketch (www.acdlabs.com). These initial structures were subsequently optimized at Hartree-Fock level using the 6-31G* basis set. The Gaussian03 program (www.gaussian.com) was used for *ab-initio* calculations. From the optimized molecular electrostatic potential, atomic partial charges were obtained using the CHELPG procedure [33]. Hence, those were scaled and adapted to the GROMOS96 force field [34]. The optimized coordinates of both the labeling fragments were modeled to link with the N_ε-nitrogens of 6 lysines (167, 344, 364, 537, 556, 586) present in the barrel interior of FhuA and 2 lysines (226, 455) at the ore of the channel. Torsion angles of the linker fragments were in the biotin-labeled fragments were adjusted manually in order to avoid clashed with side chains of other amino acids in the channel. Structures of pyridyl- and biotin-labeled FhuA were optimized subsequently in vacuum by performing a steepest descent energy minimization. The backbone of pyridyl- and biotin-labeled FhuA was keep fixed to the crystallographic position using position restraints. The molecular mechanics optimization of labeled FhuA structures were performed using Gromacs (version 3.3.1) [35, 36].

DLS Data Analysis and Results

Static and Dynamic Light Scattering were used to determine the size distribution profile of the Polymersomes in solution. Both techniques uses the intensity traces at a number of angles to derive information about the radius of gyration R_g or molecular size, molecular mass M_w, and the second virial coefficient A_2, of the molecules. In the following data the Polymersomes R_g has been measured.

4.1 Dynamic Light Scattering

4.1.1 Concentration 1 g/l

Angle	q^2 $[1/m^2]$	$1/R$ $[1/m]$	$\Delta 1/R$ $[1/m]$
30	4.687E+13	1.02E+07	-5.614074829
40	8.184E+13	1.03E+07	-5.033238367
60	1.749E+14	1.02E+07	-5.382594939
90	3.498E+14	1.08E+07	-0.438072481
130	5.747E+14	1.16E+07	7.328842695
150	6.528E+14	1.17E+07	8.689508854

Now we can compute with Excel a function which gives us the statistics for a linear graph using the method of the smallest squares, for the computation of a straight line, which is most suitable for the data, and returns a matrix, which describes the line.

$2.71307 \cdot 10^{-9}$	$9.94 \cdot 10^{6}$
$2.63272 \cdot 10^{-10}$	102994.816

With these values we can computer the maximal error

$$\Delta R = 1.04 \cdot 10^{-2}\, nm \tag{5}$$

when you plot $1/R$ $[1/m]$ over q^2 $[1/m^2]$ you get this figure.

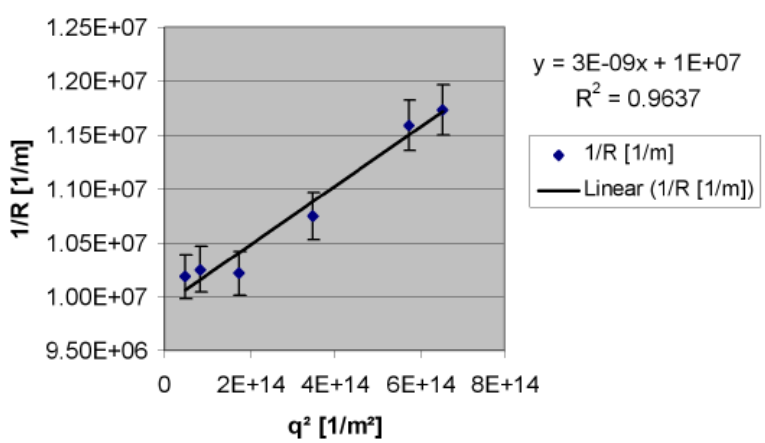

Figure 2: DLS with concentration 1 g/l

4.1.2 Concentration $\frac{1}{2}$ g/l

Angle	q^2 $[1/m^2]$	$1/R$ $[1/m]$	$\Delta 1/R$ $[1/m]$
30	4.687E+13	1.04E+07	-6.10E-02
40	8.184E+13	1.03E+07	-7.64E-02
60	1.749E+14	1.06E+07	-4.67E-02
90	3.498E+14	1.11E+07	-4.31E-03
130	5.747E+14	1.19E+07	7.31E-02
150	6.528E+14	1.22E+07	9.87E-02

Again we compute the matrix

$3.13583 \cdot 10^{-9}$	10086386.63
$2.28461 \cdot 10^{-10}$	89376.46124

With these values we can computer the maximal error

$$\Delta R = 0.008861098\, nm \tag{6}$$

when you plot $1/R$ $[1/m]$ over q^2 $[1/m^2]$ you get this figure.

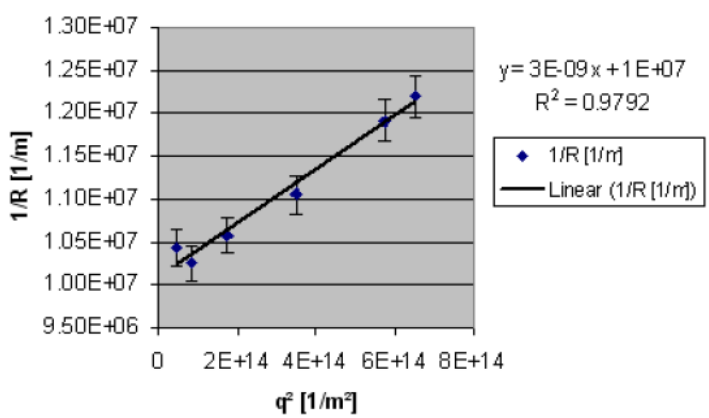

Figure 3: DLS with concentration $\frac{1}{2}$ g/l

4.1.3 Concentration $\frac{1}{4}$ g/l

Angle	q^2 $[1/m^2]$	$1/R$ $[1/m]$	$\Delta 1/R$ $[1/m]$
30	4.687E+13	9.95E+06	-1.03E-01
40	8.184E+13	1.04E+07	-6.54E-02
60	1.749E+14	1.06E+07	-4.11E-02
90	3.498E+14	1.12E+07	9.75E-03
130	5.747E+14	1.22E+07	9.73E-02
150	6.528E+14	1.22E+07	1.03E-01

Again we compute the matrix

$3.68853 \cdot 10^{-9}$	9945135.983
$2.32678 \cdot 10^{-10}$	91026.09646

With these values we can computer the maximal error

$$\Delta R = 0.009152826\, nm \tag{7}$$

when you plot $1/R$ $[1/m]$ over q^2 $[1/m^2]$ you get this figure.

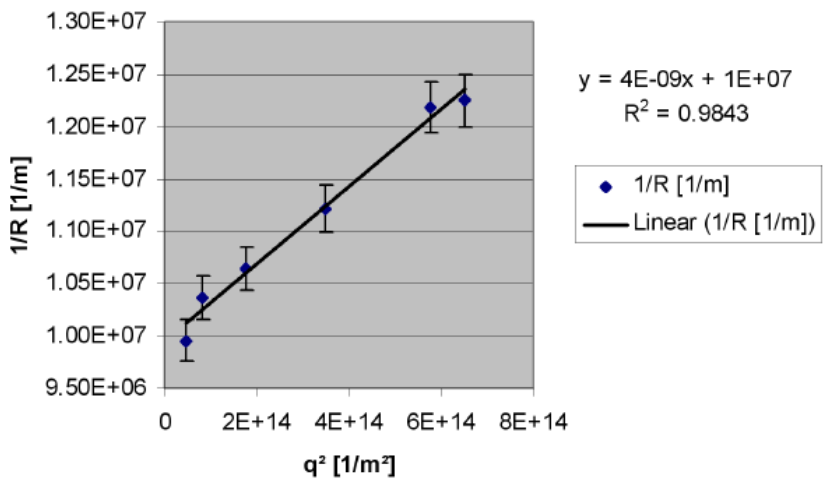

Figure 4: DLS with concentration $\frac{1}{4}$ g/l

4.1.4 Concentration $\frac{1}{5}$ g/l

Angle	q^2 $[1/m^2]$	$1/R$ $[1/m]$	$\Delta 1/R$ $[1/m]$
30	4.687E+13	1.02E+07	-8.77E-02
40	8.184E+13	1.05E+07	-6.52E-02
60	1.749E+14	1.07E+07	-4.59E-02
90	3.498E+14	1.14E+07	1.73E-02
130	5.747E+14	1.21E+07	7.65E-02
150	6.528E+14	1.25E+07	1.12E-01

Again we compute the matrix

$3.5279 \cdot 10^{-9}$	10107475.29
$1.2603 \cdot 10^{-10}$	49304.1857

With these values we can computer the maximal error

$$\Delta R = 0.004877992 nm \tag{8}$$

when you plot $1/R$ $[1/m]$ over q^2 $[1/m^2]$ you get this figure.

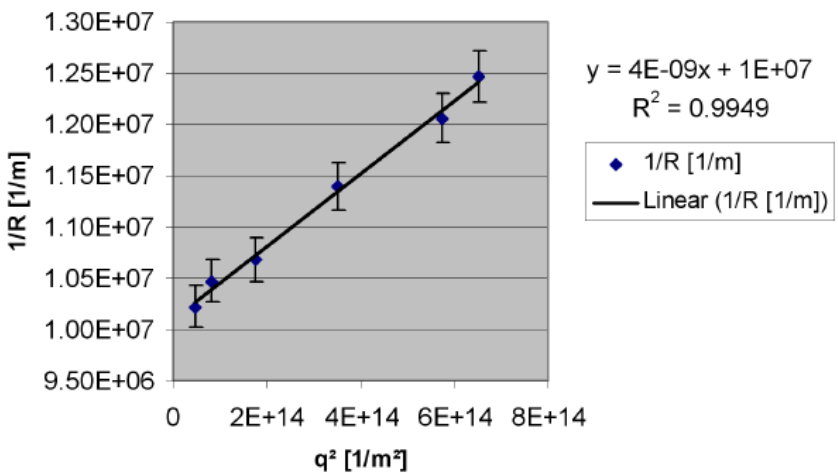

Figure 5: DLS with concentration $\frac{1}{5}$ g/l

4.1.5 Concentration $\frac{1}{8}$ g/l

Angle	q^2 $[1/m^2]$	$1/R$ $[1/m]$	$\Delta 1/R$ $[1/m]$
30	4.687E+13	8.38E+06	-2.17E-01
40	8.184E+13	9.62E+06	-1.01E-01
60	1.749E+14	1.05E+07	-1.49E-02
90	3.498E+14	1.13E+07	5.65E-02
130	5.747E+14	1.21E+07	1.35E-01
150	6.528E+14	1.24E+07	1.60E-01

Again we compute the matrix

$5.70121 \cdot 10^{-9}$	8946800.678
$9.95365 \cdot 10^{-10}$	389397.1166

With these values we can computer the maximal error

$$\Delta R = 0.043523616\, nm \tag{9}$$

when you plot $1/R$ $[1/m]$ over q^2 $[1/m^2]$ you get this figure.

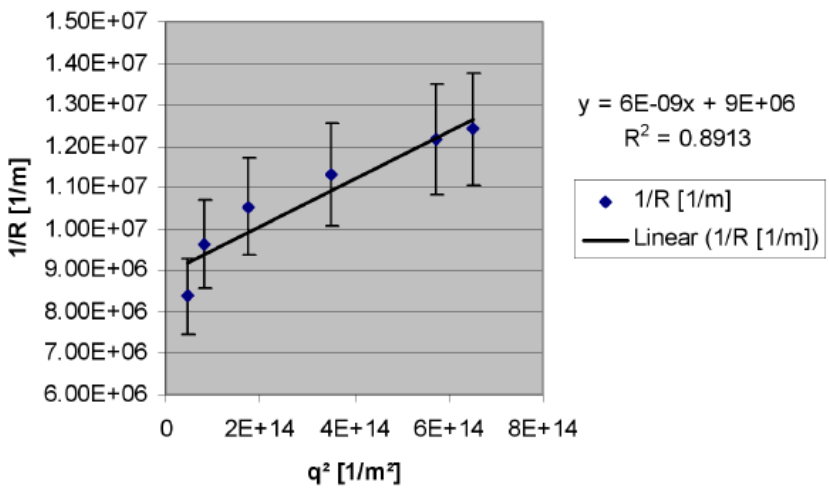

Figure 6: DLS with concentration $\frac{1}{8}$ g/l

4.1.6 Concentration $\frac{1}{10}$ g/l

Angle	q^2 $[1/m^2]$	$1/R$ $[1/m]$	$\Delta 1/R$ $[1/m]$
30	4.687E+13	9.19E+06	-1.57E-01
40	8.184E+13	9.68E+06	-1.12E-01
60	1.749E+14	1.07E+07	-1.88E-02
90	3.498E+14	1.15E+07	5.48E-02
130	5.747E+14	1.22E+07	1.16E-01
150	6.528E+14	1.23E+07	1.31E-01

Again we compute the matrix

$4.8735 \cdot 10^{-9}$	9398529.027
$6.87735 \cdot 10^{-10}$	269049.0288

With these values we can computer the maximal error

$$\Delta R = 0.028626717\, nm \tag{10}$$

when you plot $1/R$ $[1/m]$ over q^2 $[1/m^2]$ you get this figure.

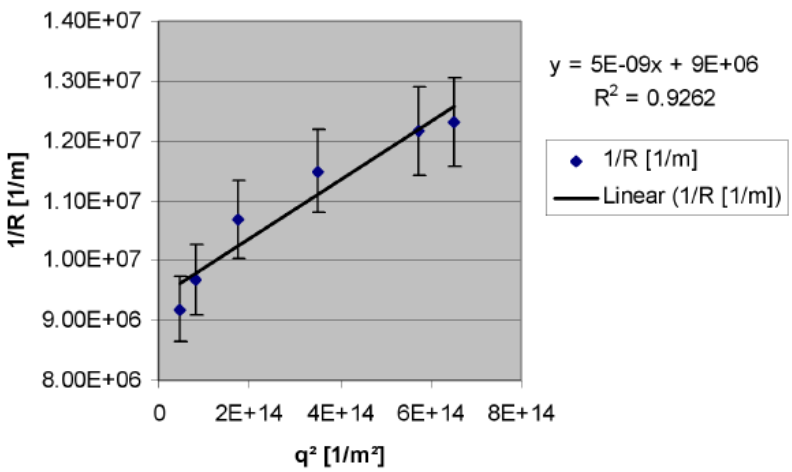

Figure 7: DLS with concentration $\frac{1}{10}$ g/l

Conc.	$1/R$ $[1/m]$
1.00	$9.94 \cdot 10^6$
0.50	10086386.63
0.25	9945135.983
0.20	10107475.29
0.13	8946800.678
0.10	9398529.027

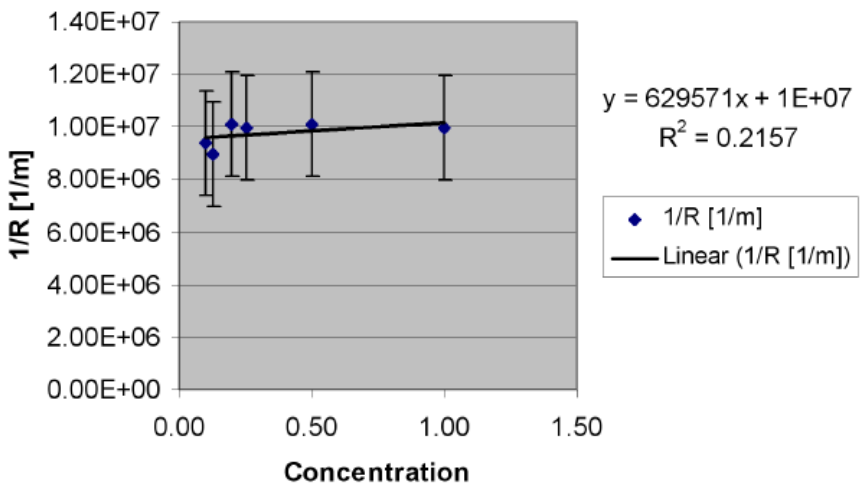

Figure 8: $1/R$ for every concentration

Again we can compute the matrix

629570.7611	9509402.105
600183.8929	287642.4747

and also the maximal error

$$\Delta R_{tot} = 0.030248219\, nm \tag{11}$$

And finally we get trough the axis intercept which is $\frac{1}{R_H}$ the hydrodynamic radius of the molecules

$$R_H = 1.05159 \cdot 10^{-7}\ m \tag{12}$$

4.2 Static Light Scattering

In static mode I measured $Kc/R\,(0°)$ values for angles between 30° and 150° every 3°. These values plotted over q^2 $[1/m^2]$ for every concentration looks like this

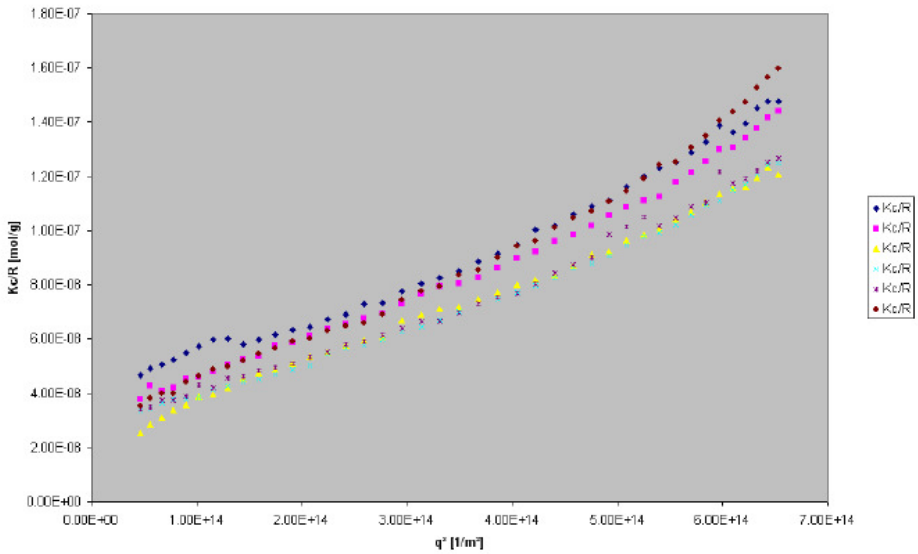

Figure 9: Kc/R for every Concentration

Again I calculated this matrix with Excel for every concentration

Concentration 1

$1.63416 \cdot 10^{-22}$	$3.42627 \cdot 10^{-8}$
$3.87089 \cdot 10^{-24}$	$1.54675 \cdot 10^{-9}$

Concentration $\frac{1}{2}$

$1.65148 \cdot 10^{-22}$	$2.70631 \cdot 10^{-8}$
$3.08411 \cdot 10^{-24}$	$1.23236 \cdot 10^{-9}$

Concentration $\frac{1}{4}$

$1.50959 \cdot 10^{-22}$	$2.09705 \cdot 10^{-8}$
$1.70039 \cdot 10^{-24}$	$6.79448 \cdot 10^{-10}$

Concentration $\frac{1}{5}$

$1.46547 \cdot 10^{-22}$	$2.19378 \cdot 10^{-8}$
$2.76517 \cdot 10^{-24}$	$1.10492 \cdot 10^{-9}$

Concentration $\frac{1}{8}$

$1.49999 \cdot 10^{-22}$	$2.2945 \cdot 10^{-8}$
$3.22017 \cdot 10^{-24}$	$1.28673 \cdot 10^{-9}$

Concentration $\frac{1}{10}$

$1.91454 \cdot 10^{-22}$	$2.17728 \cdot 10^{-8}$
$4.3836 \cdot 10^{-24}$	$1.75161 \cdot 10^{-9}$

Now if we take for every concentration the value in the right upper corner (axis intercept) and plot it over the concentration and once again make a matrix formula

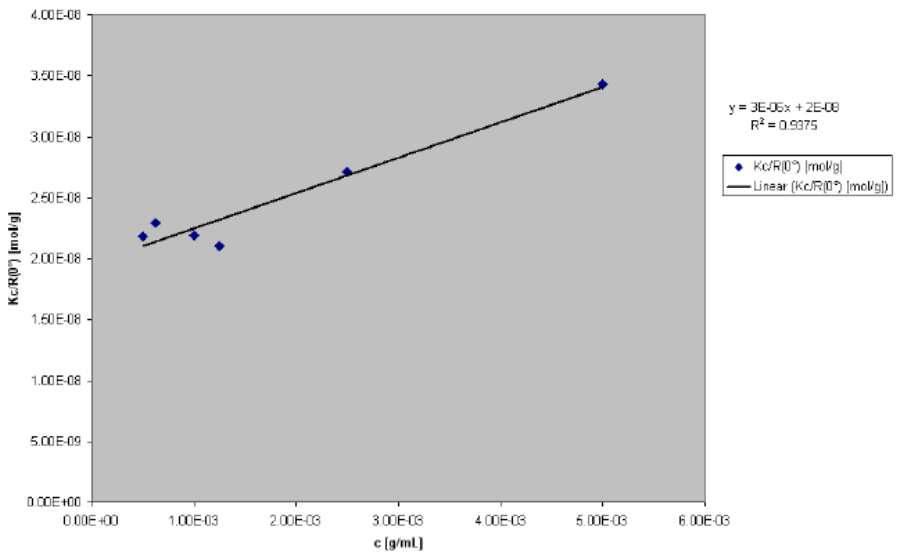

Figure 10: $Kc/R(0°)$ for every Concentration

Conc. $[g/mL]$	$Kc/R(0°)$ $[mol/g]$
$5.00 \cdot 10^{-3}$	$3.43 \cdot 10^{-8}$
$2.50 \cdot 10^{-3}$	$2.71 \cdot 10^{-8}$
$1.25 \cdot 10^{-3}$	$2.10 \cdot 10^{-8}$
$1.00 \cdot 10^{-3}$	$2.19 \cdot 10^{-8}$
$6.25 \cdot 10^{-4}$	$2.29 \cdot 10^{-8}$
$5.00 \cdot 10^{-4}$	$2.18 \cdot 10^{-8}$

$2.88627 \cdot 10^{-6}$	$1.9602 \cdot 10^{-8}$
$3.72502 \cdot 10^{-7}$	$8.9262 \cdot 10^{-10}$

The last axis intercept is exactly $\frac{1}{m}$ and with the formula

$$s = \frac{R_g^2}{3m} \tag{13}$$

We are able to calculate the gyration radius R_g

$$R_g = \sqrt{3ms} = 1.57054 \cdot 10^{-7}\ m \tag{14}$$

And the molecule radius R_m is

$$R_m = 104\ nm \tag{15}$$

With the m value we can also compute the molecules in the vesicle

$$\# = 5409.320813 \tag{16}$$

In the end we can compare the two values for R_m and R_H and we see, that they are more or less identical.

$$R_m = 105\,nm \approx 104\,nm = R_H \tag{17}$$

With this perception we have the proof that the molecules in the solution are vesicles resp. that they have a vesicular structure.

REFERENCES

[1] O. Onaca, M. Nallani, S. Ihle, A. Schenk, U. Schwaneberg, *Biotechnol J* **2006**, *1*, 795.
[2] M. Nallani, S. Benito, O. Onaca, A. Graff, M. Lindemann, M. Winterhalter, W. Meier, U. Schwaneberg, *J Biotech* **2006**, *123*, 50.
[3] W. Meier, C. Nardin, M. Winterhalter, *Angew Chem Int Ed* **2000**, *39*, 4599.
[4] C. Nardin, J. Widmer, M. Winterhalter, W. Meier, *Eur Phys J E* **2001**, *4*, 403.
[5] A. Ranquin, W. Versees, W. Meier, J. Steyaert, P. Van Gelder, *Nano Lett* **2005**, *5*, 2220.
[6] J. Ye, B. van den Berg, *Embo J* **2004**, *23*, 3187.
[7] A. D. Ferguson, V. Braun, H. P. Fiedler, J. W. Coulton, K. Diederichs, W. Welte, *Protein Sci* **2000**, *9*, 956.
[8] A. D. Ferguson, E. Hofmann, J. W. Coulton, K. Diederichs, W. Welte, *Science* **1998**, *282*, 2215.
[9] M. Braun, H. Killmann, V. Braun, *Mol Microbiol* **1999**, *33*, 1037.
[10] M. Braun, H. Killmann, E. Maier, R. Benz, V. Braun, *Eur J Biochem* **2002**, *269*, 4948.
[11] R. Koebnik, K. P. Locher, P. Van Gelder, *Mol Microbiol* **2000**, *37*, 239.
[12] M. Nallani, O. Onaca, N. Gera, K. Hildenbrand, W. Hoheisel, U. Schwaneberg, *Biotechnol J* **2006**, *1*, 828.
[13] F. Checot, J. Rodriguez-Hernandez, Y. Gnanou, S. Lecommandoux, *Biomol Eng* **2007**, *24*, 81.
[14] F. Ahmed, R. I. Pakunlu, G. Srinivas, A. Brannan, F. Bates, M. L. Klein, T. Minko, D. E. Discher, *Mol Pharm* **2006**, *3*, 340.
[15] M. Sauer, W. Meier, *Chem Comm* **2001**, *36*, 55.
[16] U. Borchert, U. Lipprandt, M. Bilang, A. Kimpfler, A. Rank, R. Peschka-Suss, R. Schubert, P. Lindner, S. Forster, *Langmuir* **2006**, *22*, 5843.
[17] A. Napoli, M. J. Boerakker, N. Tirelli, R. J. M. Nolte, N. A. J. M. Sommerdijk, J. A. Hubbell, *Langmuir* **2004**, *20*, 3487.
[18] E. G. Bellomo, M. D. Wyrsta, L. Pakstis, D. J. Pochan, T. J. Deming, *Nat Mater* **2004**, *3*, 244.
[19] P. Broz, S. Driamov, J. Ziegler, N. Ben-Haim, S. Marsch, W. Meier, P. Hunziker, *Nano Lett* **2006**, *6*, 2349.
[20] J. Carlsson, H. Drevin, R. Axen, *Biochem J* **1978**, *173*, 723.
[21] B. G. Davis, *Curr Opin Biotechnol* **2003**, *14*, 379.
[22] H. J. Schramm, T. Dulffer, *Adv Exp Med Biol* **1977**, *86A*, 197.
[23] P. Macheras, A. Iliadis, *Modeling in Biopharmaceutics, Pharmacokinetcs, and Pharmacodynamics:Homogeneous and Heterogeneous Approaches, Vol. 30*, 2006 ed., Springer, New York, **2006**.
[24] A. Prilipov, P. S. Phale, P. Van Gelder, J. P. Rosenbusch, R. Koebnik, *FEMS Microbiol Lett* **1998**, *163*, 65.
[25] P. Broz, S. M. Benito, C. Saw, P. Burger, H. Heider, M. Pfisterer, S. Marsch, W. Meier, P. Hunziker, *J Control Release* **2005**, *102*, 475.
[26] A. Graff, M. Sauer, P. Van Gelder, W. Meier, *PNAS* **2002**, *99*, 5064.
[27] C. Nardin, J. Hirt, L. Meier, W. Meier, *Langmuir* **2000**, *16*, 1035.
[28] G. T. Hermanson, *Bioconjugate Techniques*, Academic Press, New York, **1996**.
[29] G. Deleage, *DICHROPROT 2000*, Institut de Biologie et Chemie des Protéines, Lyon, **2000**.
[30] F. Thaler, M. Zamai, *Analytical Biochemistry* **2005**, *341*, 379.
[31] P. Boulanger, M. le Marie, M. Bonhivers, S. Dubois, S. Desmadril, L. Letellier, *Biochemistry* **1996**, *35*, 14216.
[32] K. P. Locher, B. Rees, R. Koebnik, A. Mitschler, L. Moulinier, J. P. Rosenbusch, D. Moras, *Cell* **1998**, *95*, 771.
[33] C. M. Breneman, K. B. Wiberg, *J Comp Chem* **1990**, *11*, 361.
[34] W. F. van Gunsteren, S. R. Billeter, E. A. A., P. H. Hünenberger, P. Krüger, A. E. Mark, W. R. P. Scott, I. G. Tironi, *Biomolecular simulation: The GROMOS96 manual and user guide*, Vdf Hochschulverlang, Zürich, Switzerland, **1996**.
[35] H. J. C. Berendsen, D. van der Spoel, R. van Drunen, *Comp Phys Comm* **1995**, *13*, 43.
[36] E. Lindahl, B. Hess, D. van der Spoel, *J Mol Model* **2001**, *7*, 306.